Universiteit
Leiden
The Netherlands

Inhibition and dynamics of a β-lactamase

Elings, W.

Citation
Elings, W. (2019, November 19). *Inhibition and dynamics of a β-lactamase*. Retrieved from https://hdl.handle.net/1887/80412

Version:	Publisher's Version
License:	Licence agreement concerning inclusion of doctoral thesis in the Institutional Repository of the University of Leiden
Downloaded from:	https://hdl.handle.net/1887/80412

Note: To cite this publication please use the final published version (if applicable).

Cover Page

Universiteit Leiden

The following handle holds various files of this Leiden University dissertation:
http://hdl.handle.net/1887/80412

Author: Elings, W.
Title: Dynamics of a β-lactamase
Issue Date: 2019-11-19

Chapter 4

Role of protein dynamics in BlaC evolution towards clavulanic acid resistance

Abstract

The β-lactamase of *Mycobacterium tuberculosis*, BlaC, is susceptible to inhibition by clavulanic acid. The ability of this enzyme to escape inhibition through mutation was probed using error-prone PCR combined with functional screening in *Escherichia coli*. The mutation that was found to confer most inhibitor resistance, K234R, together with the mutation G132N that was found previously, were then characterised *in vitro* using NMR dynamics experiments. The G132N mutant exists in two, almost equally populated, conformations that exchange with a rate of *ca*. 70 s^{-1}. The conformational change is much more prominent than in the wild type protein and affects a broader region of the enzyme, around the active site. In the K234R mutant, on the other hand, the active site dynamics were significantly diminished with respect to the wild type. These results show that multiple evolutionary routes are available to reach the inhibitor resistant phenotype in BlaC and that active site dynamics on the millisecond time scale are not required for function.

Introduction

Chemical reactions are catalysed by enzymes through stabilization of the transition state, by arranging functional groups in the active site in precise orientations with respect to the substrate. Some enzymes can have broad substrate profiles, catalysing reactions with a variety of substrates. As different substrates will have different transition states, such enzymes must have some degree of flexibility in the active site. Furthermore, in some cases a single amino acid mutation can have a profound effect on the function, switching the specificity of an enzyme from one substrate to another. Conformational dynamics are required for protein evolution, as flexibility allows promiscuity and adaptation by single amino acid substitution.[83] In this chapter, such behaviour is studied in BlaC.

Evolutionary constraints of BlaC include factors such as efficient folding and export, stability at 37 °C and the ability to break down any β-lactams that its host *Mycobacterium*

tuberculosis encounters. Such environmental constraints may change over time, requiring the protein to adapt. With increasing clinical use of β-lactam / β-lactamase inhibitor combinations for the treatment of tuberculosis, the extent to which BlaC is able to adapt to evade inhibition becomes especially interesting. Questions that are addressed here include if, how and why BlaC can evolve, through mutation of one or few amino acids, to gain resistance to the clinically most used β-lactamase inhibitor, clavulanic acid. A method was developed and executed to quickly screen around a million mutants, each carrying a combination of a few semi-random mutations in the BlaC amino acid sequence, for increased clavulanic acid resistance. Mutants that confer such resistance were identified and confirmed through further testing. On the basis of these results and those published by others in the meantime, two mutants with a single amino acid mutation each were selected and isolated. NMR dynamics studies were performed to shed light on the relation between the acquired new functions and the dynamic behaviour of the enzyme.

G132N

One of the most conserved motifs in class A β-lactamase active sites is the serine-aspartate-asparagine (SDN) motif at Ambler positions 130 – 132. In BlaC, however, the asparagine at position 132 is replaced by a glycine. This substitution effectively removes a large side chain with two functional groups from the active site pocket and thus contributes to the phenomenon that BlaC has a wider active site than most of its relatives. This wide active site, in turn, has been suggested to be important for the broad substrate profile of BlaC. Specifically, substituents at the R^6 position of carbapenem could be accommodated by this substitution.[16]

Soroka *et al.* investigated the effect of G132N mutation in BlaC.[74,75] The impact of the substitution on the hydrolysis rate differs per substrate. In BlaC, G132N increases the rates of nitrocefin, imipenem and aztreonam hydrolysis, while decreasing rates of cefoxitin and ceftazidime hydrolysis. Interestingly, however, this single mutation was found to enable BlaC to hydrolyse clavulanic acid, while simultaneously increasing the efficiency of inhibition by another inhibitor, avibactam. The same adduct masses upon reaction with clavulanate were observed for BlaC G132N as for wild type (wt), so the increased turnover must represent either impaired tautomerisation or increased hydrolysis of the tautomers. Furthermore, in at least the class A β-lactamases KPC-2, CTX-M-1 and BlaMab, like in BlaC, the Gly in this position leads to a reduced affinity for avibactam, but also to reduced stability of acyl-enzyme complex with clavulanate.[37,74,75] On the other hand, inhibition by clavulanate has been reported for many SDN-containing enzymes,[15,166,167] so the effect of this substitution appears to be very context-specific. Multiple mycobacterial β-lactamases occur in both groups.

K234R

Another conserved motif in class A β-lactamase active sites is the KTG-motif at Ambler positions 234 – 236 in the hydroxyl-binding pocket. This motif occurs in almost all class A β-lactamases, including BlaC, but not in the carbenicillin-hydrolyzing enzymes, where it is replaced by an RTG-motif. The amine of Lys234 is nested in the wall of carboxylate binding pocket, where its charge plays an important role in the electrostatic binding of the substrate. Furthermore, mutational studies have shown that it is also involved in transition state stabilization.[168] The mutation K234R was found to increase resistance to clavulanic acid in class A β-lactamases such as SHV-1[169], SHV-72[68] and SHV-84,[73] in most cases without significantly decreasing catalytic activities against penicillins. Interestingly, in another class A β-lactamase, KPC-2, the K234R mutation did not show enhanced resistance against inhibition by clavulanic acid, but it did show enhanced resistance against inhibition by avibactam.[69] MD simulations[68] and X-ray crystallography[169] have shown that the K234R mutation in SHV β-lactamases causes a displacement of the Ser130 sidechain, moving it further away from the reactive Ser70. This may prevent the cross-linking between Ser70 and Ser130, which could explain the increased resistance of the enzyme to clavulanic acid. Egesborg *et al.* have found that this mutation also confers resistance to clavulanic acid in BlaC.[73] The resistance to inhibition by clavulanic acid was shown to increase further in BlaC by combining K234R with the S130G or R220S mutations, although these mutations significantly decrease the enzymatic activity.

Results

A library of BlaC mutants was generated, harbouring on average 5 single nucleotide replacements and ~0.08 deletions per mutant (Figure S4.1a). The mutations were found to be heavily biased towards A>G/T>C and A>T/T>A mutations and against G>C/C>G, G>T/C>A and A>C/T>G mutations, with only G>A/C>T mutations having an average frequency (Figure S4.1b). This is in line with expectations, based on observations by others (e.g. [123,124]). The efficiency of the transformation was identified to be the bottleneck in library generation. Using *E. coli* strain KA797 and the transformation protocol described by Inoue *et al.*,[170] efficiencies up to 0.5 million CFU per 200 µL cell volume were obtained. More details are provided in the Supplementary text. Several million mutants, mostly harbouring multiple mutations, were screened for their ability to provide *Escherichia coli* with increased resistance to ampicillin and clavulanic acid, relatively to wt BlaC. The most promising amino acid mutations based on their frequency of occurrence and the levels of resistance they conveyed upon *E. coli* were I105V, H184R, R213S, K234R and A262V. The corresponding single amino acid mutant proteins, with the addition of the G132N mutant which had been found to hydrolyse clavulanic acid by Soroka *et al.*,[74] were produced and purified. Their respective abilities to resist inhibition by clavulanic acid were characterised by measuring the onset of inhibition by 10 µM clavulanic acid (Figure 4.1). Part of this

work for the I105V and G132N mutants was performed in cooperation with Danny van Zanten.

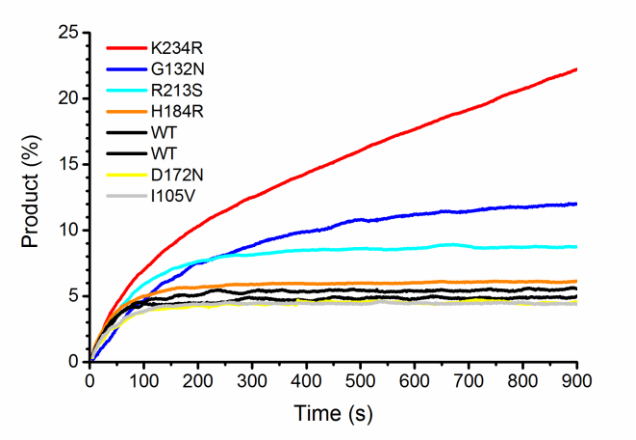

Figure 4.1. Inhibition curves of nitrocefin hydrolysis by wt BlaC and single amino acid mutants of BlaC with 10 µM clavulanic acid. The protein concentration that was used varied between the different mutants, therefore the product concentration is displayed relative to the total product that is converted by the same concentration of the same BlaC variant in 900 seconds, when it is not inhibited. Mutations D172S, R213S and K234R were found together in one mutant, as were H184R and K234R. I105V was found in combination with D42G and R277C, which were not further tested as single mutants.

The effects of the I105V, H184R and A262V mutations on inhibition were not found to be significant. As these mutations were all found in combination with others, their effects may be epistatic or stability-related, but the more obvious explanation would be that the mutations are random, without any functional effect. This was not further investigated. The R213S mutant was found to require about four-fold more time than wt BlaC to reach full inhibition. This mutation may decrease the affinity of BlaC for clavulanate somewhat. The G132N and K234R mutations were found to convey more inhibition resistance, maintaining some level of activity even after prolonged exposure. As discussed before, both of these mutants had already been identified by others and have been well-characterised kinetically. However, nothing is known about the dynamic behaviour of these enzymes. To study this, the $^{1}H^{15}N$ spectra of BlaC mutants G132N and K234R were recorded and assigned through comparison of their HNCa spectra to that of wt BlaC. In the wt spectrum, peaks have been assigned to all non-proline backbone amides except Asp2 and four phosphate-binding residues in the active site.[28] The mutant proteins each exhibited well-dispersed spectra that show significant overlap with the wt spectrum, indicating that both share the same overall fold with wt BlaC (Figure S4.2).

In the spectrum of K234R BlaC, peaks were assigned to all the backbone amide groups that were assigned in wt BlaC, including Arg234. Also the resonance belonging to the backbone

amide of Thr235 could be assigned. This resonance is not detectable in the spectrum of wt BlaC (Figure S4.2, marked with *).

In the spectrum of G132N BlaC, many resonances could not be detected. The region for which peaks of backbone amides have broadened beyond detection was found to have extended from the four phosphate-binding residues in wt BlaC to include Glu166, the active site-covering loop ranging from Ser104 to Val108 and the loop between helices 6 and 7, containing Ser130 and the variant residue Asn132 (Figure 4.2). Surprisingly, this last stretch of undetectable amides extends all the way until Leu137, spanning half of helix 7 (Figure 1.3). Furthermore, the resonances of several surrounding residues were observed to have split between two positions. These observations indicate the presence of a chemical exchange process. The split peaks have a minimum distance of ~21 and ~24 Hz in the ^{1}H and ^{15}N dimensions, respectively, which means that the rate of exchange between the two states must be lower than *ca.* 100 s^{-1}. The relative peak intensities of the split peaks suggest populations of *ca.* 60 and 40 %. In the protein structure, the amides for which the resonances were broadened or split are centred around the G132N mutation and the rest of the active site (Figure 4.2).

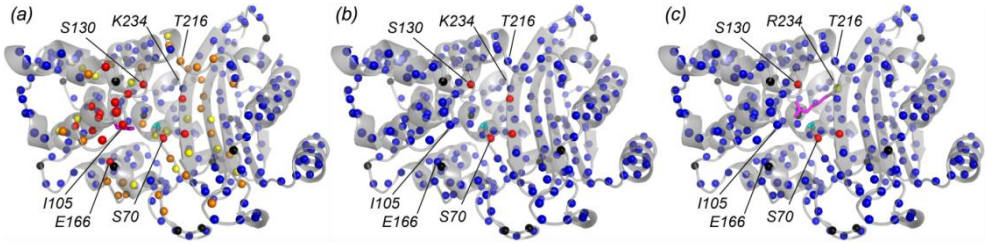

Figure 4.2. Residues for which the backbone amide resonances were lost, split or diminished in the spectra of *(a)* G132N, *(b)* wt and *(c)* K234R. Backbone amides are indicated as spheres. Red: no resonance could be assigned. Orange: two resonances assigned. Yellow: one resonance assigned, but peak intensity diminished below half of the wt relative peak intensity. Blue: one resonance assigned, normal peak intensity. Black: proline. The Ser70 side chain is indicated as a cyan stick, mutant side chains are indicated as magenta sticks, modelled into subunit A of the structure with PBD entry 5NJ2.[28]

The positions of the backbone amide resonances in the spectra of both mutants were compared with those of wt BlaC (Figure 4.3). Large and extensive chemical shift perturbations (CSP) were observed for both mutants, which we attribute to significant disturbances of the active site water network close to the mutation site, as well as in the extended hydrogen bonding network. No large perturbations were observed for any residues that are very far from the mutation site in the wt structure, further corroborating that the proteins are correctly folded.

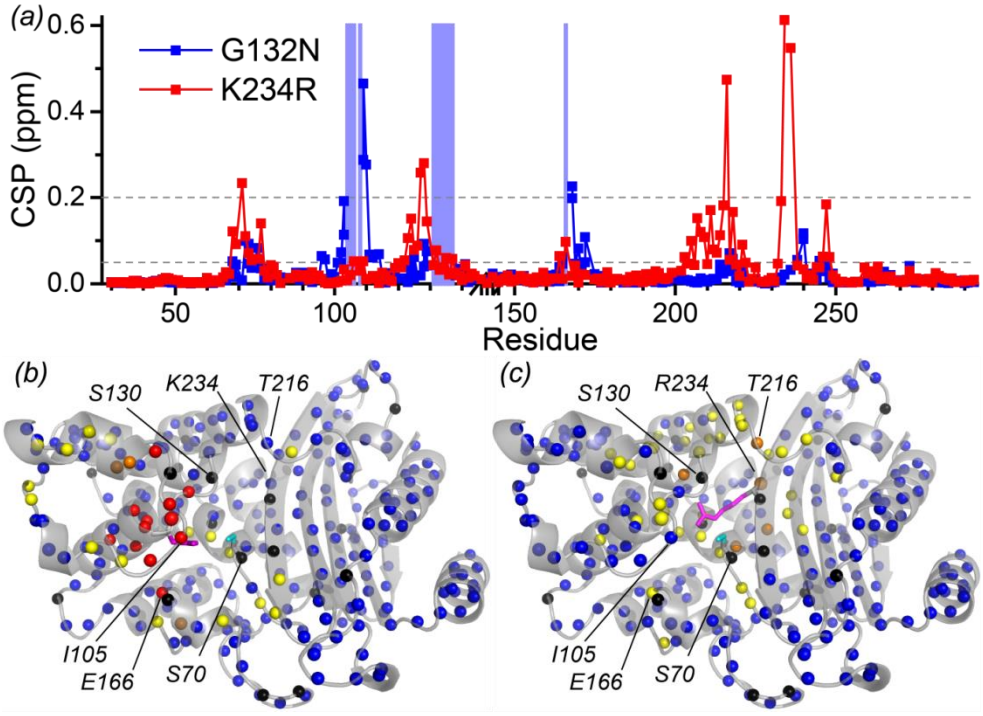

Figure 4.3. Chemical Shift Perturbation (CSP) of BlaC backbone amide resonances upon mutation. *(a)* Plot of average absolute CSP on the sequence [|½Δδ(^{1}H)| + |0.1*Δδ(^{15}N)|]. Blue background indicates residues that have broadened beyond detection in the G132N mutant. Grey dashed lines represent cut-off values for the colouring of amides in *(b).* The break on the horizontal axis represents the insertion of a G-G-G-T-loop, relative to Ambler numbering. Error bars have been omitted for clarity, estimated 95% confidence interval is ± 0.03 ppm. *(b, c)* Plot of CSP for BlaC G132N *(b)* and BlaC K234R *(c)* on the structure. Orange: CSP > 0.2 ppm. Yellow: 0.2 ppm ≥ CSP > 0.05 ppm. Blue: CSP ≤ 0.05 ppm. Red: Peak broadened beyond detection in G132N but not in wt BlaC. Black: no data available. Side chains of the mutated residues are displayed in magenta stick representation. Structure: PBD entry 5NJ2, subunit A.

As the K234R mutation is very near to the phosphate binding site and appears to affect the dynamic behaviour of at least Thr235, which participates in phosphate binding, the phosphate affinity was measured with a titration. Surprisingly, a K_D of 20.1 ± 0.7 mM (Figure S4.3, error from fit of one titration) was found for BlaC K234R, which is close to the K_D of 27 ± 11 mM (error from duplicate titration) found for wt BlaC (Figure 2.5, [28]).

To probe the effect of these mutations on the pico- to nanosecond dynamics, the Nuclear Overhauser Effect (*NOE*) of the backbone amides was measured (Figure 4.4). The high *NOE*s indicate that the two mutants, like wt BlaC, are overall very rigid. The *NOE*s of most residues are very similar to wt, showing the expected reductions for flexible loops and high values in long β-sheets and α-helices. There are also residues that show increased or decreased rigidity. Notably, residue Ile247 in K234R displays a very low *NOE*. This amide is

situated on β-strand 4, directly adjacent to residue 234 on β-strand 3. In the wt structure, the Ile247 amide is hydrogen bonded to the carbonyl group of Lys234. The loss of rigidity that we observe may suggest that this hydrogen bond is lost upon mutation of Lys234 to Arg. However, the other amides on these two strands show *NOE*s that are similar to those in wt, indicating that the effect is very local. In G132N, fast dynamics are observed around Ser70, at least for one of the two forms. Val80, which displays increased flexibility in wt BlaC, is stabilised in G132N and even further in K234R, where it returns to a normal rigidity compared to the rest of the protein.

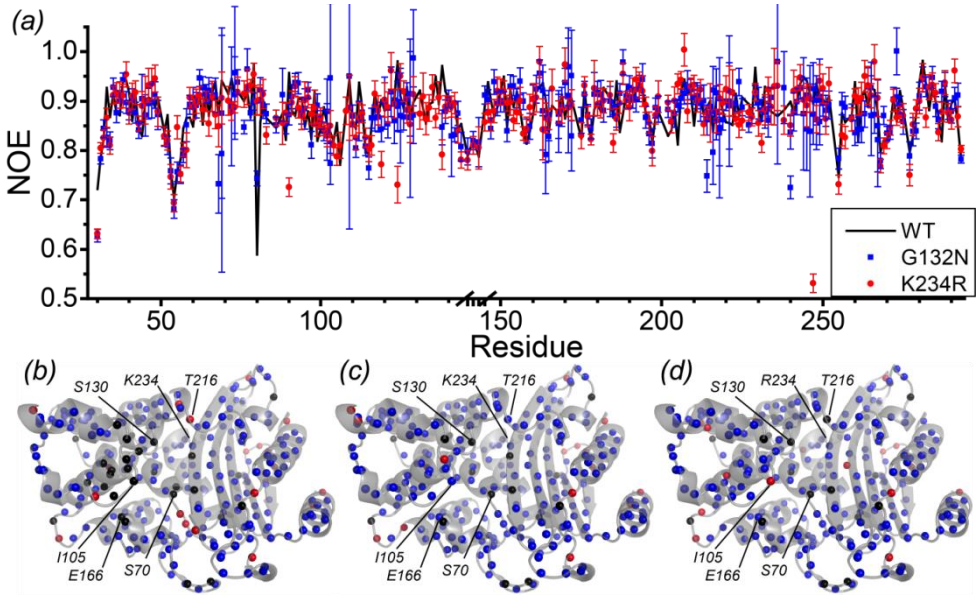

Figure 4.4. Nuclear Overhauser Effect (*NOE*) of mutant and wt backbone amides. *(a)* Plot of *NOE* for each residue. The break on the horizontal axis represents the insertion of a G-G-G-T-loop, relative to Ambler numbering. Error bars indicate the standard deviation based on the spectral noise. The wt BlaC *NOE* values are displayed as a line for reference, values and errors can be found in Figure 3.2 and under BMRB ID 27888. Mutant *NOE* values are also included under BMRB IDs 27889 (G132N) and 27891 (K234R). *(b-d)* Plots of *NOE* values on the BlaC structure, for G132N *(b)*, wt *(c)* and K234R BlaC *(d)*. Backbone amides with *NOE* < 0.8 are displayed in red, those with *NOE* ≥ 0.8 in blue and those for which no data are available in black. Structure: PDB entry 5NJ2, subunit A.

To probe the effect of the G132N and K234R mutations on the millisecond dynamics of BlaC, CPMG relaxation dispersion experiments were performed. In wt BlaC, significant relaxation dispersion was observed around the active site, indicating dynamics with an exchange rate of *ca.* 860 s^{-1} (Chapter 3 and Figure 4.5a, black). Surprisingly, this relaxation dispersion is completely absent in mutant K234R (Figure 4.5a, red). The opposite effect is observed in mutant G132N, which shows strikingly increased relaxation dispersion for many residues (Figure 4.5a, blue). Like the broadened and split peaks, the peaks that show

relaxation dispersion are also centred around the active site (Figure 4.5b). A few example CPMG profiles are provided in Figure 4.6 and more in Figure S4.4.

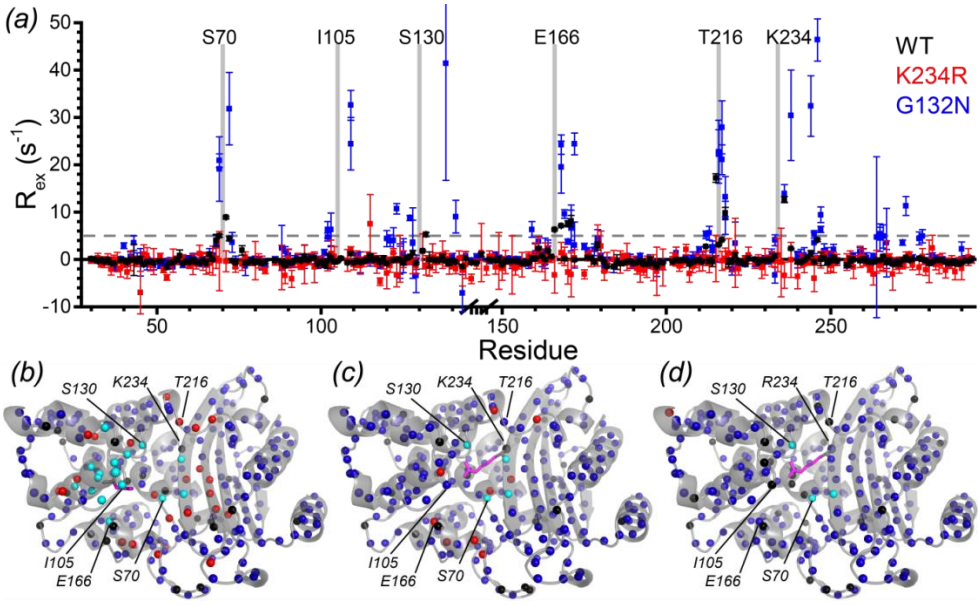

Figure 4.5. Chemical exchange effects observed for backbone ^{15}N resonances in BlaC, as measured by CPMG relaxation dispersion analysis. R_{ex} is defined as the $R_{2,eff}$ at ν_{CPMG} = 25 s^{-1} minus that at 1000 s^{-1}. *(a)* Plot of R_{ex} vs. the residue number. The break on the horizontal axis represents the insertion of a G-G-G-T-loop, relative to Ambler numbering. Error bars represent the 95% confidence interval based on three duplicate delays per experiment. Values can also be accessed under BMRB IDs 27888 (wt), 27889 (G132N) and 27891 (K234R). *(b)-(d)* Colour map of R_{ex} on the structure, for G132N *(b)*, wt *(c)* and K234R BlaC *(d)*. Backbone amides with R_{ex} > 5 s^{-1} are displayed in red and those with R_{ex} ≤ 5 s^{-1} in green. Amides for which the resonance was broadened beyond detection are displayed in cyan. Amides for which no data was available for a different reason (e.g. proline or too much overlap) are displayed in black. Mutated residues are displayed as magenta sticks, modelled into subunit A of the structure with PBD entry 5NJ2.[28]

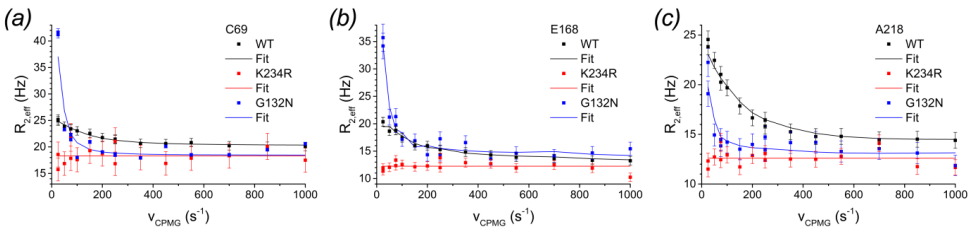

Figure 4.6. Example CPMG profiles from BlaC wt, G132N and K234R. The lines represent global fits using CATIA software for BlaC wt and G132N and individual fits to $R_{2,eff}$ = c for BlaC K234R. Error bars represent standard deviation based on three duplicate frequencies.

A global fit using CATIA software[97] of 36 G132N dispersion profiles (Figure S4.4) resulted in an estimate of the exchange rate of 70 ± 2 s^{-1}, and the state B population (p_B) of 48.99 ± 0.01 %. This fitting procedure also yields the absolute ^{15}N chemical shift difference, $|\Delta\Omega|$, between the resonance positions of the two states. For several residues, the fitted $|\Delta\Omega|$ is significantly larger than the coalescence point at an exchange rate of 70 s^{-1}, which is ~0.18 ppm at the experimental magnetic field strength of 20 T. This implies that these amides are predicted to experience slow-intermediate exchange. This, together with the extraordinarily high predicted p_B, means that the fit predicted that the second states of these peaks should be visible in the spectrum. As we did indeed observe doubled peaks, we were able to cross-check the fit by comparing the predicted $|\Delta\Omega|$ values with those that were measured in the spectrum assignment (Figure 4.7). The fitted and observed $|\Delta\Omega|$ values correlate well, though there appears to be a small bias, reflecting either an experimental underestimation of $|\Delta\Omega|$ due to peak picking artefacts of partly overlapping peaks, or an overestimation of the $|\Delta\Omega|$ by the fitting procedure. However, the results clearly suggest that the observed peak doubling reflects the same exchange process as observed with the RD experiments.

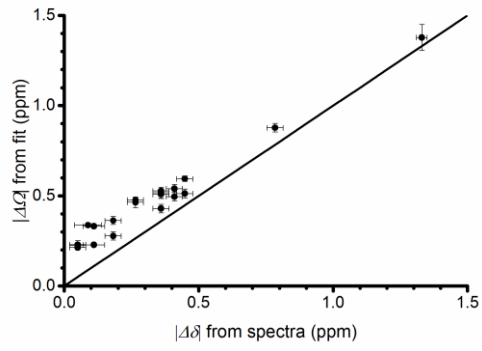

Figure 4.7. Correlation plot of the |ΔΩ| derived from RD NMR versus the ^{15}N chemical shift differences observed in the HSQC-spectrum for the two BlaC G132N states. The diagonal line indicates y=x. Vertical and horizontal error bars represent standard deviation of the fit and the estimated error in the peak picking, respectively.

Chemical exchange with a rate of 70 s^{-1} should also be observable using the Chemical Exchange Saturation Transfer (CEST) method. We previously reported no measurable exchange in this regime for wt BlaC. CEST of the G132N mutant was measured, yielding direct observation of exchange between the resonances with the largest chemical shift differences, Gly238 and Asp246 (Figure S4.5). Unfortunately, the $|\Delta\Omega|$ values of the other exchanging resonances are too small to be observed clearly via CEST. No other CEST profiles indicated exchange. Nevertheless, it is clear that the doubled peaks in the G132N spectrum arise from two states of the protein that are in exchange.

The exchange rate and excited state population (p_B) of 70 s^{-1} and 49 %, respectively, were obtained from a global fit of as many similar relaxation dispersion profiles as possible, as is the usual practice. Usually, however, only state A is visible and can be measured directly. In the BlaC G132N spectrum, both states are visible and a mix of the two were used in the fit. Although this procedure does yield the most accurate estimate of the exchange rate, the estimate of the p_B can obviously not be trusted. Fortunately, the facile detection of the two states allows us to determine which peaks correspond to the same populations by simply acquiring TROSY-HSQC's at various temperatures. The relative intensities of ten non-overlapping peak pairs at five temperatures ranging from 279 to 298 K were used to determine that the true population of state B at 298 K is 40 ± 2 %. Furthermore, this analysis revealed that the major state at 298 K becomes the minor state at lower temperatures and thus has a higher energy level (Figure 4.8). The CATIA relaxation dispersion fit was repeated for states A and B separately, with p_b fixed at 0.4 and 0.6, respectively. This yielded exchange rates and $|\Delta\Omega|$ values that are very similar to those from the global fit (Figure S4.6).

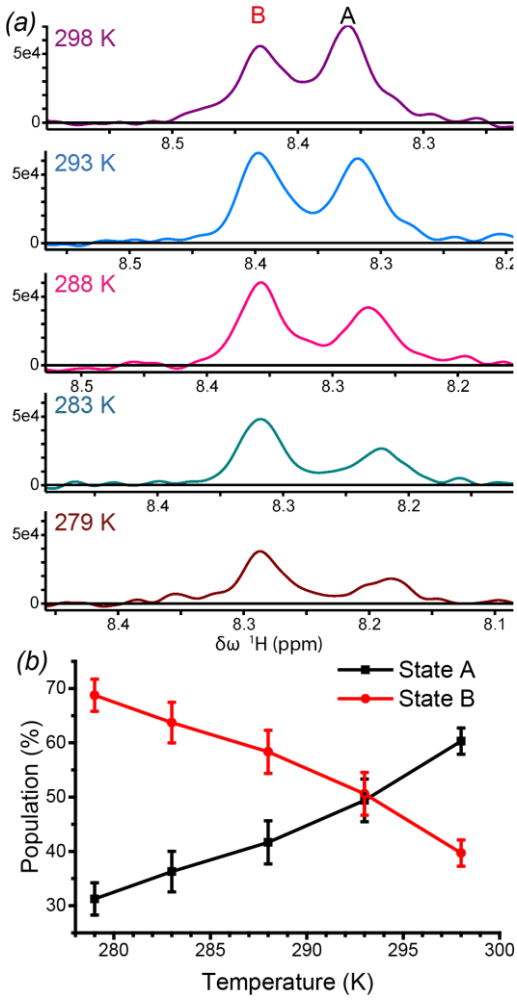

Figure 4.8. Temperature dependence of BlaC G132N state B population. *(a)* Example of a doubled peak, Ala164, at five temperatures. The $|\Delta\Omega|$ in the ^{15}N dimension is zero for this amide, as is the ^{15}N $\Delta\delta$ in the temperature titration, thus slices through this dimension yield the peak shapes and maxima for both states A and B. Note that peak maxima normally decrease with temperature as a result of sample viscosity. *(b)* Average and standard deviation of relative intensities of ten split backbone amide resonances in the five ^{1}H-^{15}N TROSY-HSQC spectra.

Discussion

Here we reported on the dynamics of two variants of BlaC that both increase resistance to inhibition by clavulanic acid. Curiously, the mutations have opposite effects on the dynamic behaviour in the millisecond time scale. K234R reduces the active site chemical exchange in the millisecond time scale, while G132N increases it. Neither mutation has large effects on the pico- to nanosecond time scale dynamics of BlaC.

G132N

We show that BlaC G132N exists in two almost equally populated states, exchanging with a rate of *ca.* 70 s^{-1}. This is observed through the splitting of backbone amide resonance peaks around the active site and the mutation, as well as through CEST and relaxation dispersion experiments. Additionally, the resonances of amides in a large region around the mutation have broadened beyond detection. However, it should be noted that several very broad peaks in the two-dimensional TROSY-HSQC spectra remain unassigned due to being undetectable in the three-dimensional HNCa spectrum. Generally, most of the active site resonances that are detectable have broadened significantly in the HNCa and thus barely reach the detection threshold. These observations, combined with the concentric localisation of the peak broadening, the peak splitting and the relaxation dispersion, suggest that all of these effects may arise from the same exchange process with a rate of 70 s^{-1} and a state B population of 40 % at 298 K.

The observed chemical exchange of BlaC G132N is significantly slower than the active site exchange process that was observed for the wt protein, *ca*. 860 s^{-1} (Chapter 3), and it is detected in a much broader region of the protein. The observations of broadened and split resonance peaks rather parallel those for wt BlaC bound to clavulanic acid. Upon inhibitor binding, resonances are also lost or split into multiple peaks, in a very similar region of the protein (compare Figure 4.2a, Figure 3.7). Chemical exchange between the split peaks in bound form, like in the G132N mutant, must be much slower than the exchange that wt BlaC displays in free form. However, although the protein region that is affected by peak splitting is very similar in the two cases, the relative positions in which the split peaks appear in the spectrum are not. Furthermore, in the G132N spectrum, resonances that split all show two states with consistent exchange and relative populations. This is not the case for inhibitor-bound BlaC, where for one of the amides, three resonance positions could be identified. Moreover, the large relaxation dispersion that we observe for G132N amides is absent in inhibitor-bound wt protein. Therefore, although the observations in the two datasets are reminiscent, it seems unlikely that they represent the same dynamic process.

To interpret the process, it is important to consider the effect of the G132N mutation. The Asn side chain introduces a relatively large extra moiety in the active site of BlaC. This requires spatial adaptation of other residues that occupy the same position, most notably Ser104. This residue in wt BlaC points inwards to take the space that is occupied by Asn132 in TEM-1 and SHV-1, where the residue at position 104 points outward (Figure 4.9). Intuitively, a minor dislocation of the loop that covers the active site like a lid appears to be the most accessible way to generate space for the Asn side chain. Indeed, in TEM-1, this loop is located a few Å further away from the active site (Figure 4.9).

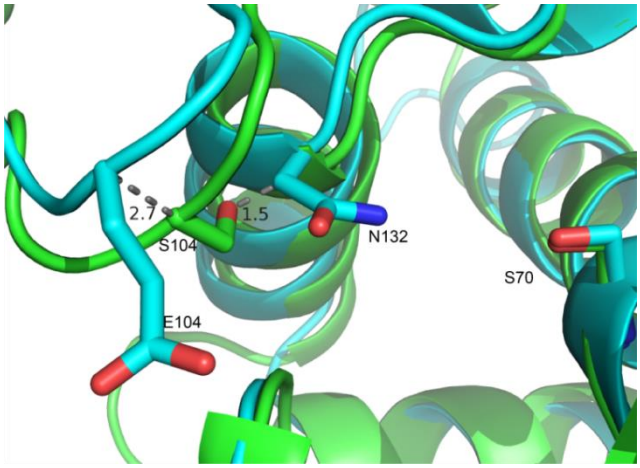

Figure 4.9. Alignment of BlaC (green) with TEM-1 (cyan). TEM-1 Asn132, Glu104 and BlaC Ser104 as well as both Ser70 residues are displayed in stick representation. Dashed grey lines indicate distances in Å. In BlaC, Ser104 would clash with an Asn residue at position 132. In TEM-1, residue 104 is displaced relative to Ser104 in BlaC. The distance between the C_α atoms is 2.7 Å.

A dislocation of the 'lid' loop would presumably affect the hydrogen bonds between the lid loop and residues 131-134 (Figure 4.10), in line with the NMR effects observed for these residues (Figure 4.3 and Figure 4.5). Unless displacement of the lid loop involves partial unfolding of helix 7, it does not explain, however, why the resonances of amides 135 – 137 have also broadened beyond detection. The reason for this may lie in an interaction between Asn132 and Glu166. A reorientation of the backbone at position 166 could drastically change the chemical environment of Asn136, which staples the omega loop to the α-domain via hydrogen bonds with the backbone carbonyl and amide of Glu166 (Figure 4.10). In fact, movement of the tip of the omega-loop into and out of the active site is the commonly held model for the active millisecond dynamics that are observed in several class A β-lactamases, including BlaC (Chapter 3).

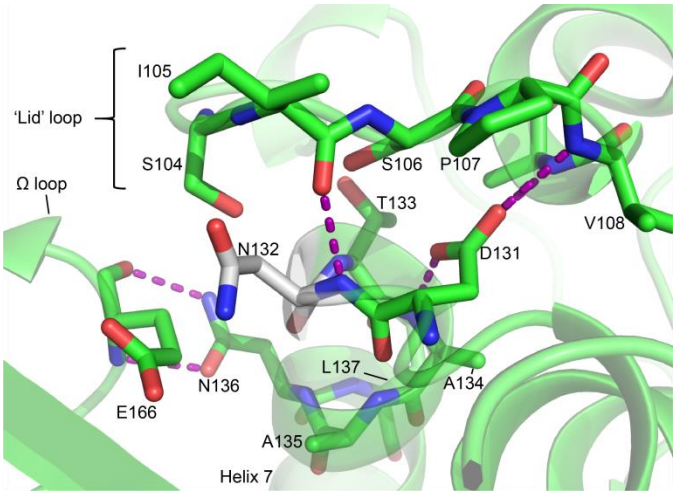

Figure 4.10. View of the BlaC active site with Asn132 modelled into a similar position that it takes in TEM-1. BlaC (PDB 5NJ2[28]) is displayed in transparent cartoon representation, with several residues that are mentioned in the text in stick representation. Several hydrogen bonds are indicated with purple dashed lines (all are 2.7 – 2.9 Å).

The question remains if the exchange process is involved in the functional differences between the enzyme and the mutant, increased clavulanate resistance and avibactam affinity, or if it is an unrelated side effect of the mutation. The protein exists in two almost equally populated states that interconvert slowly, and we cannot simply assume that the two states have equal properties. In the simplest model, the two observed states are similar to the two states that wt BlaC exhibits (Chapter 3). If it is assumed that one state hydrolyses clavulanic acid and binds avibactam much better than the other state, then the G132N mutation favours the former state. In this model, the 140-fold increase in carbamylation rate of avibactam observed by Soroka *et al.*[75] for G132N BlaC compared to the wt enzyme could be explained if the population of this active state changed from *ca.* 0.3 or 0.4 % in wt to 40 or 60 % in G132N, respectively. However, such a low population of the excited state in the wt BlaC is not in line with the NMR results. The population of the minor state in the wt enzyme must sizable to completely broaden the resonances of the four active site residues, as was discussed in Chapter 3. Furthermore, if the same state is also responsible for the increased hydrolysis of clavulanic acid acyl adduct, then the turnover rate of clavulanic acid should increase by the same factor 140. Soroka *et al.* found a k_{cat} of clavulanate hydrolysis by BlaC G132N of 0.4 ± 0.1 s^{-1} in 100 mM MES pH 6.4 at 293 K. The hydrolysis of clavulanate by wt BlaC was not detected in their experiments, but we have found turnover rates up to 2.3 (± 0.2) 10^{-4} s^{-1} in the same buffer at 298 K (Chapter 2, [28]). This difference is almost an order of magnitude larger than the factor 140 in apparent avibactam affinity. Clearly, the functional effects of the G132N mutation cannot solely be explained by the increased population of state B. The insertion of an Asn

sidechain must change the shape and electronegativity of the active site surface. Even without dynamics, this could contribute to the altered functionality of the enzyme. For example, it is interesting to note that in structures of BlaC bound to avibactam, there is a gap between the active site wall containing Gly132 and the adduct (Figure 4.11a). Tassoni *et al.* have shown that this gap allows the avibactam adduct to rotate slightly away, releasing the sulphate moiety from the hydroxyl-binding pocket (Figure 4.11b). In SHV-1, which has a much higher affinity for avibactam than BlaC,[74,171] this gap is filled by the Asn132 sidechain. It may be that the shape of the BlaC binding pocket is simply not a very good match for avibactam and the G132N mutation increases affinity. Furthermore, the displacement of Ser104 and presumably the whole loop including gatekeeper residue Ile105 may make the binding site more accessible for avibactam.

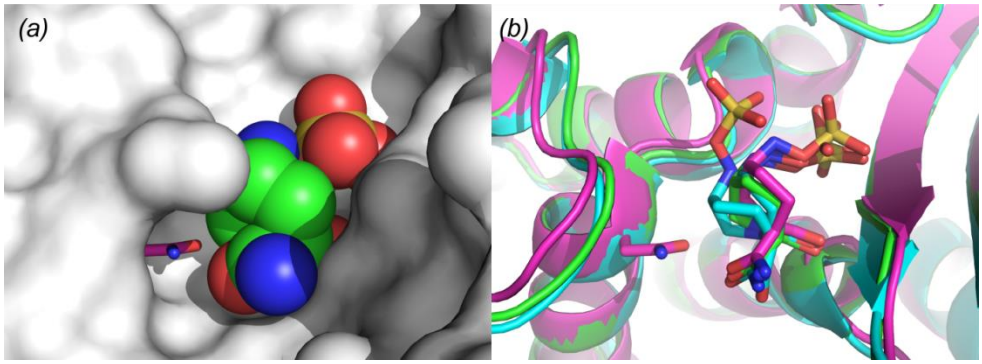

Figure 4.11. BlaC bound to avibactam. *(a)* The BlaC active site in surface representation bound to avibactam in spacefilling representation (PDB 4df6[41]). A gap is visible in between the adduct and the enzyme. In the gap, the Asn132 side chain of SHV-1 bound to avibactam (PDB 4zam[172] aligned to 4df6) is visible in sticks representation. *(b)* The same viewpoint and structures (4df6 in green, 4zam in magenta) as *(a)*, with the addition of another structure of BlaC bound to avibactam (PDB 6h2h[160] in cyan). Here, all structures are displayed in cartoon representation with the avibactam adducts in sticks. Two orientations of avibactam are visible in the 6h2h BlaC structure. The smallest heavy atom centre distance between the 4zam Asn132 side chain and the 6h2h normal avibactam orientation is 3.0 Å, while that between Asn132 and the tilted avibactam orientation is only 2.2 Å. This suggests that this avibactam orientation may not occur in BlaC G132N.

Further research will be required to elucidate the role of dynamics in clavulanate hydrolysis by BlaC G132N. However, the question of whether such dynamics are required to reach this phenotype in BlaC can be answered conclusively via comparison to another clavulanate-resistant mutant.

K234R

The dynamic behaviour of wt BlaC on the millisecond time scale (Chapter 3) is not detectable in mutant K234R. This indicates that the millisecond chemical exchange is not required for clavulanate hydrolysis. Moreover, as this mutant is able to hydrolyse at least ampicillin, bezylpenicillin, cephalothin[73] and nitrocefin, it forms direct evidence that the millisecond dynamics are not required for β-lactamase activity. Doucet *et al.* first reported

changes in millisecond dynamics in TEM-1 to correlate with functional differences,[103] but later observed that a laboratory-engineered chimeric β-lactamase displayed conserved function but strikingly increased dynamic behaviour.[111] To our knowledge, however, BlaC K234R is the first functional class A β-lactamase in which no millisecond dynamics could be detected in or near the active site. It is important to note, however, that the inability to detect such dynamics does not mean that no dynamics are present. An important indicator of the dynamic behaviour of the class A β-lactamases is the broadening of some of the resonances of their active site backbone amides. In BlaC, four of these amides are broadened beyond detection. While mutant K234R is the first BlaC variant in which the Thr235 backbone amide could be identified, we have still been unable to identify the resonances for the amide groups of Ser70, Ser130 and Thr237. These missing peaks suggest that an exchange process is still present, most likely too fast to probe using CPMG relaxation dispersion experiments (~ 50 – 3000 s^{-1}) but too slow to affect the *NOE* (~ 10^9 – 10^{12} s^{-1}). Such dynamics could possibly be measured using an $R_{1,rho}$ spin-lock experiment (~ 10^3 – 10^6 s^{-1}) or detected through residual dipolar couplings (~ 10^3 – 10^{12} s^{-1}), but such experiments are outside the scope of this thesis.

Materials and methods

Error-prone PCR

Error-prone PCR mutagenesis was performed on an *Escherichia coli*-expression optimised DNA sequence (Figure S4.7) encoding the soluble domain of BlaC, using DreamTaq polymerase (0.1 U/µL, ThermoFisher Scientific), using the reaction conditions as recommended by the supplier but disturbed by the addition of manganese (0.2 mM), extra magnesium (2 mM) and skewed nucleotide concentrations (0.52 mM dCTP/dTTP vs 0.2 mM dATP/dGTP) in the reaction mixture. The primers that were used are listed in Table S4.1. Fifteen rounds of error-prone PCR were followed by purification of the reaction product using the Illustra GFX PCR DNA and Gel Band Purification Kit (GE LifeSciences) and another 25 rounds of non-error-prone PCR to further amplify the product. Primers for the second PCR (Table S4.1) anneal only to the product of the first reaction, not to the template. The product of the second PCR was purified as before and subsequently digested using restriction enzymes *Bgl*II and *Xho*I, with addition of *Dpn*I to digest any original template. The resulting gene fragments, containing only the coding sequence of soluble BlaC with semi-random combinations of mutations, were purified by agarose gel band extraction. These were subsequently cloned into similarly digested and purified pUK21-based vectors containing expression and subcellular localisation elements to create a cloning/expression plasmid capable of IPTG-induced expression of BlaC mutants fused to an N-terminal, TorA-derived protein export signal for use in *E. coli*. A map of the construct is shown in Figure S4.8. These plasmids were introduced into *E. coli*

strain KA797[173] using the chemical transformation method described by Inoue *et al*.,[170] yielding libraries of up to 0.5 million CFU per 200 µL transformation. Screening for clavulanate resistance was performed by incubating at 37 °C overnight on LB agar containing 50 µg/mL kanamycin sulfate, 1 mM IPTG, 8 µg/mL ampicillin and 1 µg/mL clavulanic acid. Colonies were transferred to separate liquid cultures and after overnight incubation, plasmids were isolated from the cells and used to transform fresh cells. Hits were only registered as valid if the plasmid also transmitted the same ampicillin/clavulanic acid-resistant phenotype to the fresh cells. Mutation frequency and bias in the library were controlled by Sanger sequencing of at least 10 randomly picked colonies from plates without ampicillin and clavulanic acid.

Site-directed mutagenesis

Site-directed mutations in the *blaC* gene, encoding the amino acid sequence as detailed in Figure S2.3, were made using a whole-plasmid synthesis approach, with the primers listed in Table S4.1. Incorporation of the correct mutations and absence of any other mutations was checked by comparison of Sanger sequencing data of each mutant from two sides (Baseclear BV, Leiden).

Protein production and purification

Pure BlaC of wt and mutants, without signal peptide and without purification tag, but with an N-terminal Gly residue instead of a Met (sequence as in Figure S2.3), was obtained as described previously (Chapter 2, [28]). The Ambler standard β-lactamase numbering scheme[17] is used throughout this thesis.

NMR spectroscopy

All NMR spectra were recorded on a Bruker AVIII HD 850 MHz (20 T) spectrometer equipped with a TCI cryoprobe. Unless mentioned otherwise, all experiments were performed on samples containing 0.38 mM ^{15}N enriched BlaC in 94 mM MES/NaOH pH 6.4 and 6% D_2O, at 298 K. HNCa spectra were measured on samples containing 0.6 and 0.28 mM $^{15}N^{13}C$ enriched BlaC G132N and K234R, respectively, in the same buffer. These spectra were recorded using the standard Bruker pulse program 'trhncaetgp3d', processed with Topspin 3.2 (Bruker Biospin, Leiderdorp) and analysed using CCPNmr Analysis.[143] Residue assignment of the peaks was performed by comparison of the HNCa to the assigned wt spectra (Chapter 3, BMRB ID 27888) and can be accessed under BMRB IDs 27889 for BlaC G132N and 27891 for BlaC K234R. *NOE* measurements were performed using standard Bruker pulse program 'hsqcnoef3gpsi' with a ^{1}H saturation delay of 4 s. *NOE* data were processed with Topspin 3.2 and resulting peak heights were fitted to exponential decay curves using Dynamics Center 2.5 (Bruker BioSpin, Rheinstetten).

CPMG relaxation dispersion measurements were performed using the TROSY CPMG pulse program as detailed by Vallurupalli *et al.*,[163] with 0, 1 (2x), 2, 3 (2x), 4, 6, 8, 10 (2x), 14, 18,

22, 28, 34 and 40 ^{15}N 180˚ pulses in 40 ms relaxation time, respectively. Data were processed with NMRPipe[164] and resulting resonances were fitted to a glore lineshape using FuDa.[97] Effective transverse relaxation rates ($R_{2,eff}$) were calculated from the fitted peak heights using an exponential decay function. Chemical exchange rate and p_B were determined using a grouped fit with the software CATIA.[97]

Chemical Exchange Saturation Transfer (CEST) measurements were performed using the standard Bruker "hsqc_cest_etf3gpsitc3d" pulse program, with 2.5 s recycle delay and 0.8 s B_1 irradiation at all frequencies in the ^{15}N range 100.5:0.5:130 ppm and field powers of 8 Hz and 26 Hz.

Figures containing protein structures were created using the PyMOL Molecular Graphics System, Version 2.2 Schrödinger, LLC.

Supplementary text

Optimisation of the library generation pipeline

The digestion / ligation approach was compared to Gibson Assembly (in-house), the InFusion Cloning Kit (Takara, Inc.) and the GeneMorph® II EZClone Domain Mutagenesis Kit (Agilent Technologies). The in-house digestion / ligation approach was chosen because it outscored the other approaches in the number of transformed mutants per transformation. The most efficient insert : vector ratio for ligation and subsequent transformation was found to be 3 or 4 : 1 (Figure S4.9). Strain KA797 was found to be the most efficient strain for transformation that was available in-house. Surprisingly, chemical transformation was found to yield more transformants than electrotransformation did. Commercial XL10-Gold cells were found to be ~3x more competent than KA797 cells when the latter were prepared via the standard in-house chemically competent cell preparation protocol, but an order of magnitude less than KA797 cells prepared via the 'Simple and Efficient Method' (SEM) described by Inoue *et al*.[170] (Table S4.2). Strain KA797 was also found to be a useful strain for library screening (Table S4.3). An ampicillin concentration of 8 µg/mL was found to be the minimum required concentration to prevent any non-resistant KA797 cell from forming a colony on the plate after transformation. Likewise, 1 µg/mL clavulanic acid was found to be enough to inhibit colony formation of all wild type BlaC expressing cells. When incubated at room temperature (with 1 mM IPTG), KA797 cells that were transformed with the BlaC cloning/expression plasmid were only resistant to ~2 µg/mL ampicillin (*vs*. ~16 µg/mL at 37 °C). Pre-induction with IPTG or switching to *E. coli* strain DH5α did not increase this MIC. Screening for mutants with increased clavulanic acid resistance but decreased temperature stability was therefore not attempted. Several of these optimisation experiments were performed in cooperation with Ralphe Drenth.

Supplementary figures

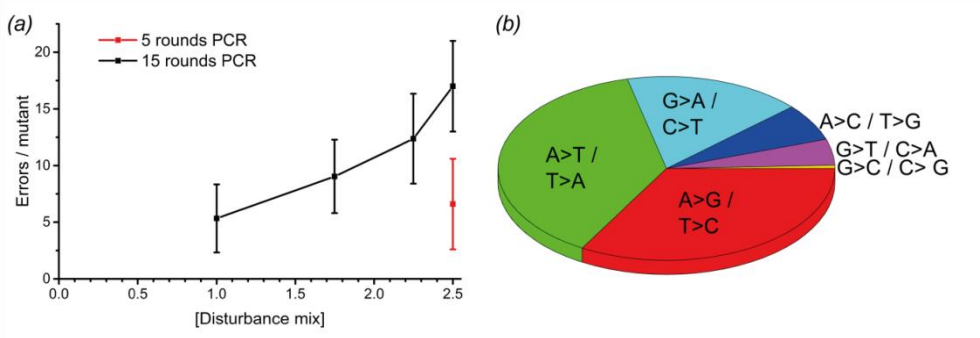

Figure S4.1. Semi-random mutagenesis. *(a)* Mutation frequency average and standard deviation as a function of the concentration of 'disturbance mix' consisting of 0.2 mM manganese, 2 mM extra magnesium and 0.32 mM extra dCTP/dTTP. Fifteen rounds of PCR with 1x disturbance mix was used for generation of the library. *(b)* Mutation bias, based on 369 single basepair replacements.

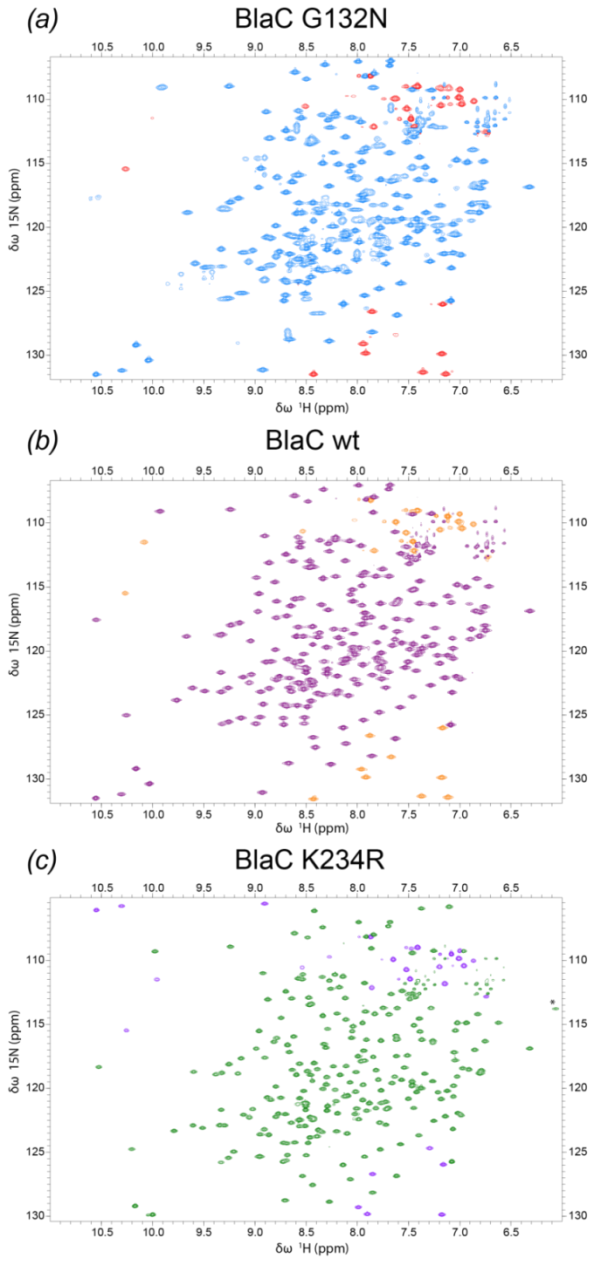

Figure S4.2. TROSY-HSQC spectra of BlaC wt and mutants. In each case, contour levels in the minority colour indicate folded peaks. Assignments can be accessed under Biological Magnetic Resonance Bank ID 27889. The resonance marked with an * in the BlaC K234R spectrum is assigned to the Thr235 amide.

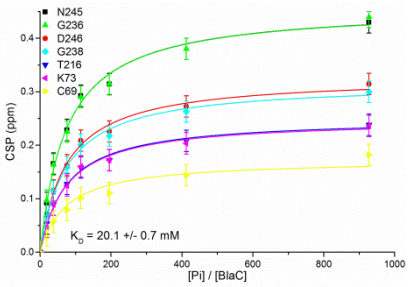

Figure S4.3. BlaC K234R – phosphate binding curves. The plot shows the CSPs upon phosphate titration for seven selected backbone amide resonances plotted against the ratio of the phosphate and BlaC concentrations. Data points are shown with an estimated peak picking error of ±0.02 ppm, error in K_D is the standard error of the global fit.

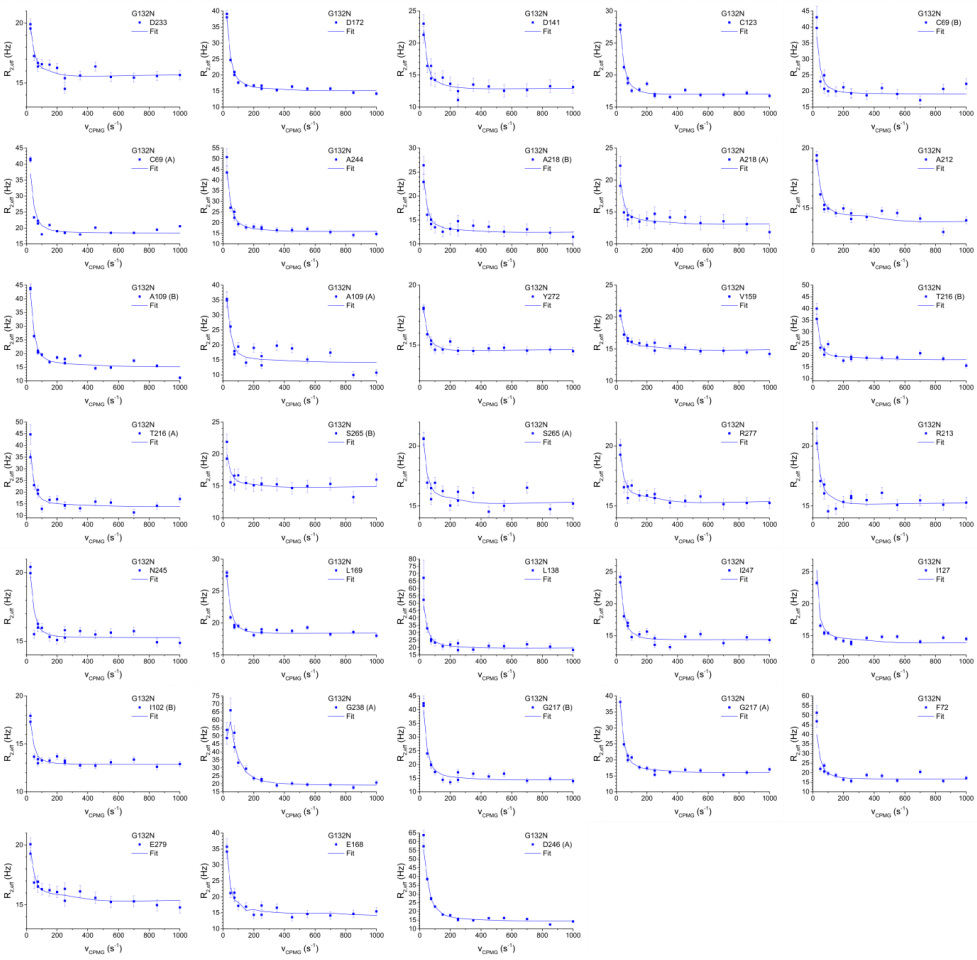

Figure S4.4. Relaxation dispersion curves of G132N backbone amides, with global fit. Error bars represent the standard deviation based on three duplicate CPMG frequencies.

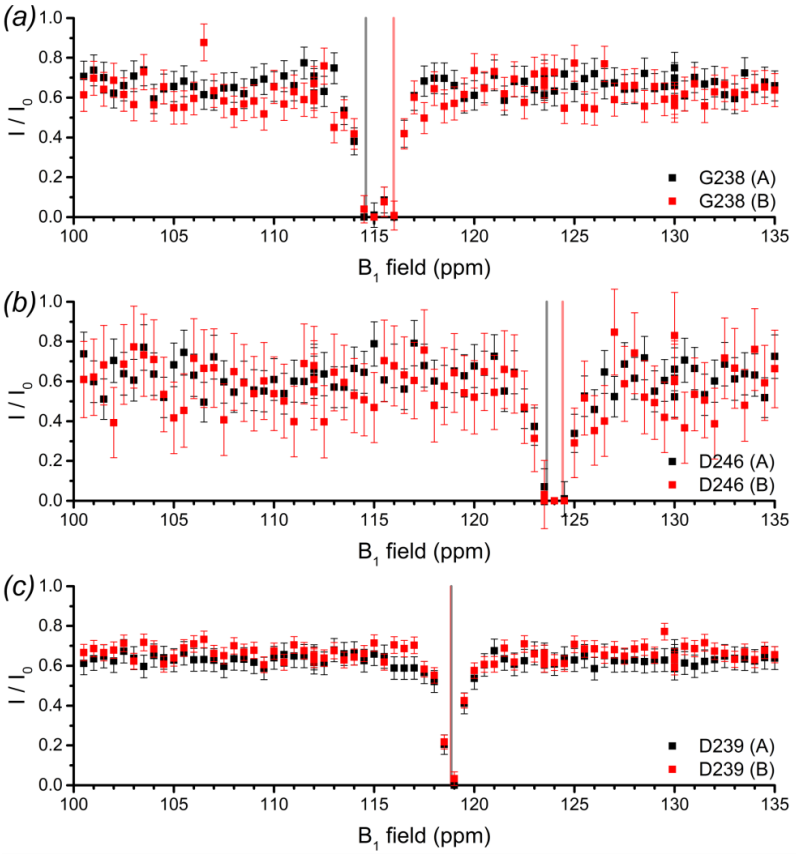

Figure S4.5. CEST profiles of G132N backbone amides Gly238 *(a)*, Asp246 *(b)* and Asp239 BlaC *(c)*. Vertical bars represent the peak positions of state A (black) and B (red). In panels *(a)* and *(b)*, the ^{15}N chemical shift difference between states A and B is large and exchange between the states can be observed via broadening of the two saturation dips. Panel *(c)* is included for reference, here the observable ^{15}N chemical shift difference between states A and B is small and the exchange is therefore not detectable. All other profiles (not shown) have profiles that are similar to *(c)*. Error bars indicate the standard deviation based on the spectral noise. These errors, especially those in *(b),* are very large due to the splitting and broadening of the peaks.

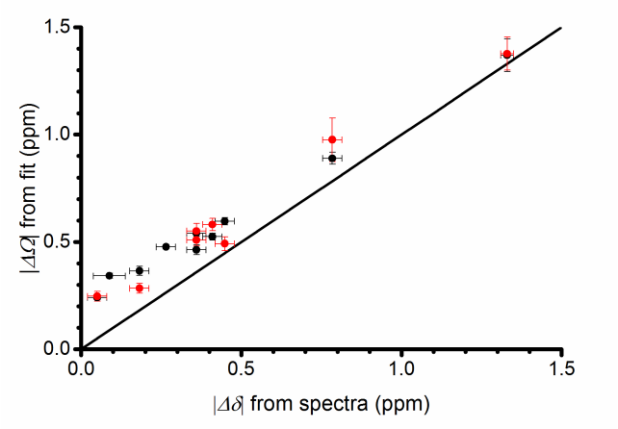

Figure S4.6. Correlation plot of the |ΔΩ| derived from relaxation dispersion NMR fits of the separate states A (black) and B (red) versus the ^{15}N chemical shift differences observed in the HSQC-spectrum for the two BlaC G132N states. The diagonal line indicates y=x. Y error bars represent standard deviation of the fit, x error bars represent estimated error in the peak picking. These fits were performed with p_b fixed at 0.4 and 0.6, respectively. The fit of state A relaxation dispersion data yielded an exchange rate estimate of 82 ± 3 s^{-1} and that of state B yielded 77 ± 5 s^{-1}.

ATG*gccaataatgacctgtttcaggcaagccgtcgtcgttttctggcacagctgggtggtctgaccgt*
*tgcaggtatgctgggtccgagcctgctgacaccgcgtcgtgcaaccgcagcacaggca*GATCTGGCAG
ATCGTTTTGCAGAACTGGAACGTCGTTATGATGCACGTCTGGGTGTTTATGTTCCGGCAACCGGCACC
ACCGCAGCAATTGAATATCGTGCAGATGAACGTTTTGCATTTTGCAGCACCTTTAAAGCACCGCTGGT
TGCAGCCGTTCTGCATCAGAATCCGCTGACCCATCTGGATAAACTGATTACCTATACCAGTGATGATA
TCCGTAGCATTAGTCCGGTTGCACAGCAGCATGTTCAGACCGGTATGACCATTGGTCAGCTGTGTGAT
GCAGCAATTCGTTATAGTGATGGCACCGCAGCCAATCTGCTGCTGGCCGATCTGGGTGGACCGGGTGG
TGGTACAGCAGCCTTTACCGGTTATCTGCGTAGCCTGGGTGATACCGTTAGCCGTCTGGATGCAGAAG
AACCGGAACTGAATCGTGATCCGCCTGGTGATGAACGTGATACCACCACACCGCATGCCATTGCACTG
GTTCTGCAGCAGCTGGTTCTGGGTAATGCACTGCCTCCGGATAAACGTGCACTGCTGACCGATTGGAT
GGCACGTAATACCACCGGTGCCAAACGTATTCGTGCAGGTTTTCCGGCAGATTGGAAAGTTATTGATA
AAACCGGTACGGGTGATTATGGTCGTGCAAATGATATTGCAGTTGTTTGGAGCCCGACCGGTGTTCCG
TATGTTGTTGCAGTTATGAGCGATCGTGCCGGTGGTGGCTATGATGCCGAACCGCGTGAAGCACTGCT

Figure S4.7. Sequence of the BlaC gene that was used for generation of the mutant library. Bases in upper case encode the BlaC protein, lower case italics encodes the TorA-derived protein export signal for use in *E. coli*, lower case without italics encodes a C-terminal 6-histidine purification tag.

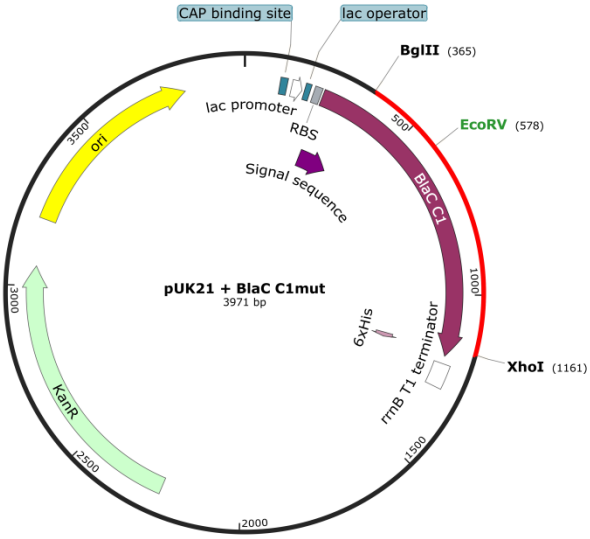

Figure S4.8. Map of the cloning/expression plasmid used for generation of the mutant library. The section of DNA that was mutated through error-prone PCR is displayed in red.

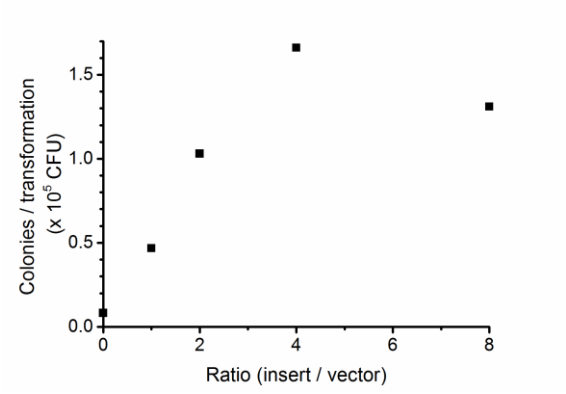

Figure S4.9. Transformation efficiency as a function of ligation condition.

Supplementary tables

Table S4.1. Primers that were used in this study. Bases that are displayed in red indicate mutations with respect to the wild type sequence.

Process	Primer sequences (5' - 3')
Error-prone PCR	GCTAGCTCAGTCCTAGGTATAATGCTAGCGTTTAACTTTAAGAAGGAGATATACCATGG; CCCGGGAGCTCGAATTCCCTCAGTGGTGGTGGTGGTGGTG
Second amplification	CGCCACGGCGATATCGGATCCTTGACAGCTAGCTCAGTCCTAGGTATAATGC; CCCGGGAGCTCGAATTCCC

G132N mutagenesis	GCAGCAATTCGTTATAGTGATAACACCGCAGCCAATCTGCTGC; GCAGCAGATTGGCTGCGGTGTTATCACTATAACGAATTGCTGC
K234R mutagenesis	GCAGATTGGAAAGTTATTGATAGAACCGGTACGGGTGATTATGG; CCATAATCACCCGTACCGGTTCTATCAATAACTTTCCAATCTGC
I105V mutagenesis	GTGATGATATCCGTAGCGTTAGTCCGGTTGCACAGC; GCTGTGCAACCGGACTAACGCTACGGATATCATCAC
R213S mutagenesis	GCTGACCGATTGGATGGCAAGTAATACCACCGGTGCCAAACG; CGTTTGGCACCGGTGGTATTACTTGCCATCCAATCGGTCAGC
H184R mutagenesis	CGTGATACCACCACACCGCGTGCCATTGCACTGGTTCTGC; GCAGAACCAGTGCAATGGCACGCGGTGTGGTGGTATCACG
D172N mutagenesis	GCAGAAGAACCGGAACTGAATCGTAATCCGCCTGGTGATGAACG; CGTTCATCACCAGGCGGATTACGATTCAGTTCCGGTTCTTCTGC

Table S4.2. Transformation efficiency of SEM competent *E. coli* KA797 as a function of DNA concentration. This test was performed with intact plasmids. The approximate amount of DNA per transformation that was used for the library generation is indicated in bold.

Plasmid (ng)	CFU ($\times 10^4$)	CFU / Plasmid molecule ($\times 10^{-5}$)	CFU / cell ($\times 10^{-4}$)
0.125	2	70	3
1.25	29	100	40
12.5	***142***	**50**	**200**
42.5	177	20	200
85	331	20	500
170	341	9	500
425	461	5	600
850	625	3	800

Table S4.3. Ampicillin Minimal Inhibitory Concentration (MIC) for several *E. coli* strains with and without BlaC. Plates were grown overnight at 37 °C in the presence of 1 mM IPTG, after application of 150 µL of cultures with 30 minutes pre-induction and cell density OD_{600} = 10.

Strain	**Ampicillin MIC (µg/mL)**	
	- BlaC	**+ BlaC**
KA797	2	32
BL21 Codon+	0.5	16
BL21 pLys CPF	0.5	16
BL21 STAR (DE3) pLys	1	32
BL21 pLysE	0.5	0.5
BL21 pLysS	0.5	64